Supplementary Material

Accounting for uncertain fault geometry in earthquake source inversions – I: theory and simplified application

Théa Ragon[1], **Anthony Sladen**[1] **and Mark Simons**[2]

[1] Université Côte d'Azur, CNRS, Observatoire de la Côte d'Azur, IRD, Géoazur, 250 rue Albert Einstein, 06560 Valbonne, France.
[2] Seismological Laboratory, California Institute of Technology, 1200 E. California Blvd., Pasadena, CA 91125, USA.

1 Influence of uncertainty on fault dip for an optimization approach

As in the Bayesian approach (Section 3.2), we assume a fault with a 20 km down-dip extent that prolongs infinitely along strike, and with a true dip of 55° for the dip-slip case we investigate. The 100 data points follow an irregular distribution and are calculated from a uniform target slip model of 1 meter from the surface to 20 km down dip. To precompute the prediction covariance matrix, we use the result of the optimization neglecting $\mathbf{C}_\mathrm{p}$ as initial model (see Section 2.3.1). We perform a non-negative least squares inversion and include spatial smoothing following the approach of Tarantola (2005). The choice of regularization parameters is explained in Fig. S9.

The inferred parameters and their posterior uncertainty $\mathbf{C}_\mathrm{m} = (\mathbf{G}^T \cdot \mathbf{C}_\chi^{-1} \cdot \mathbf{G})^{-1}$ are presented in Fig. 12. Similarly to the Bayesian tests, the ability of the optimization algorithm to approach the target slip model depends on the inclusion of $\mathbf{C}_\mathrm{p}$. If the assumed fault geometry is incorrect and related uncertainties not accounted for (Fig. 12a), the inferred model is at odds with the target model. Conversely, the inclusion of $\mathbf{C}_\mathrm{p}$ in the optimization allows the quasi-perfect approximation of the target model (Fig. 12b). Comparably to the Bayesian approach, the posterior uncertainty of model parameters increases with depth. For shallowest subfaults, posterior uncertainty is limited. Yet, for deeper subfaults, posterior PDFs become quasi-uniform, similarly to the Bayesian case. This large posterior uncertainty comes from the depth limited model resolution of our fault parametrization (Tarantola, 2005; Menke, 2012). The closer the model resolution is to 1 for a subfault, the better the model is resolved. For our 20-subfaults parametrization, the model resolution falls to almost 0 at depth (Figs 12a,b). To compensate for this limited resolution, a possibility is to increase the size of subfaults (as discussed in Pritchard et al., 2002; Page et al., 2009) which allows to have a model resolution close to 1 everywhere on the fault (Figs 12c,d). Figs 12(c) and (d) show the resulting slip models for a fault discretization coarsening with depth from 1 km-wide subfaults at the surface, to 2 km-wide subfaults and then to 4 km-wide subfaults on the deepest parts of the fault. In this case, the impact of an incorrect fault geometry on inferred parameters is lower (Fig. 12c) as the problem becomes less under-determined. With $\mathbf{C}_\mathrm{p}$ included, the posterior uncertainty is even more reduced and the target model is approached with an uncertainty that does not exceed 20 cm (Fig. 12d). We could use the same approach to reduce the posterior uncertainty of Bayesian estimations. Qualitatively, the predictions of surface displacement for both models including and neglecting $\mathbf{C}_\mathrm{p}$ are identical to the Bayesian approach predictions. RMS of residuals between observations and predictions are smaller for models neglecting $\mathbf{C}_\mathrm{p}$ than for models including $\mathbf{C}_\mathrm{p}$: 1.1 mm, 2.5 mm and 0.66 mm respectively for strike-perpendicular, strike-parallel and vertical displacements with no $\mathbf{C}_\mathrm{p}$, while the almost perfectly solved slip distribution with $\mathbf{C}_\mathrm{p}$ has RMS of 2.6 mm, 3.7 mm and 1.9 mm. These RMS values are about 2 mm less than the ones found with a Bayesian inversion. Indeed, with the optimization approach, the inversion is based on the minimization of the misfit between observations and predictions. Instead, with a Bayesian approach the misfit is part oflikelihood and the algorithm is not strictly driven by misfitmization. Additionally, the RMS calculated in the Bayesian case is based on the posterior mean model, and not the model minimizing the misfit. Whatever the source inversion method employed, we show that the inclusion of a dip uncertainty covariance matrix in the inversion is critical to retrieve a more realistic slip distribution model.

References

Menke, W., 2012. *Geophysical data analysis: Discrete inverse theory*, Academic press.

Page, M. T., Custódio, S., Archuleta, R. J., & Carlson, J. M., 2009. Constraining earthquake source inversions with GPS data: 1. Resolution-based removal of artifacts, *Journal of Geophysical Research: Solid Earth*, **114**(B1), B01314.

Pritchard, M. E., Simons, M., Rosen, P. A., Hensley, S., & Webb, F. H., 2002. Co-seismic slip from the 1995 July 30 Mw= 8.1 Antofagasta, Chile, earthquake as constrained by InSAR and GPS observations, *Geophysical Journal International*, **150**(2), 362–376.

Tarantola, A., 2005. *Inverse Problem Theory and Methods for Model Parameter Estimation*, Other Titles in Applied Mathematics, Society for Industrial and Applied Mathematics.

2 Supplementary Figures

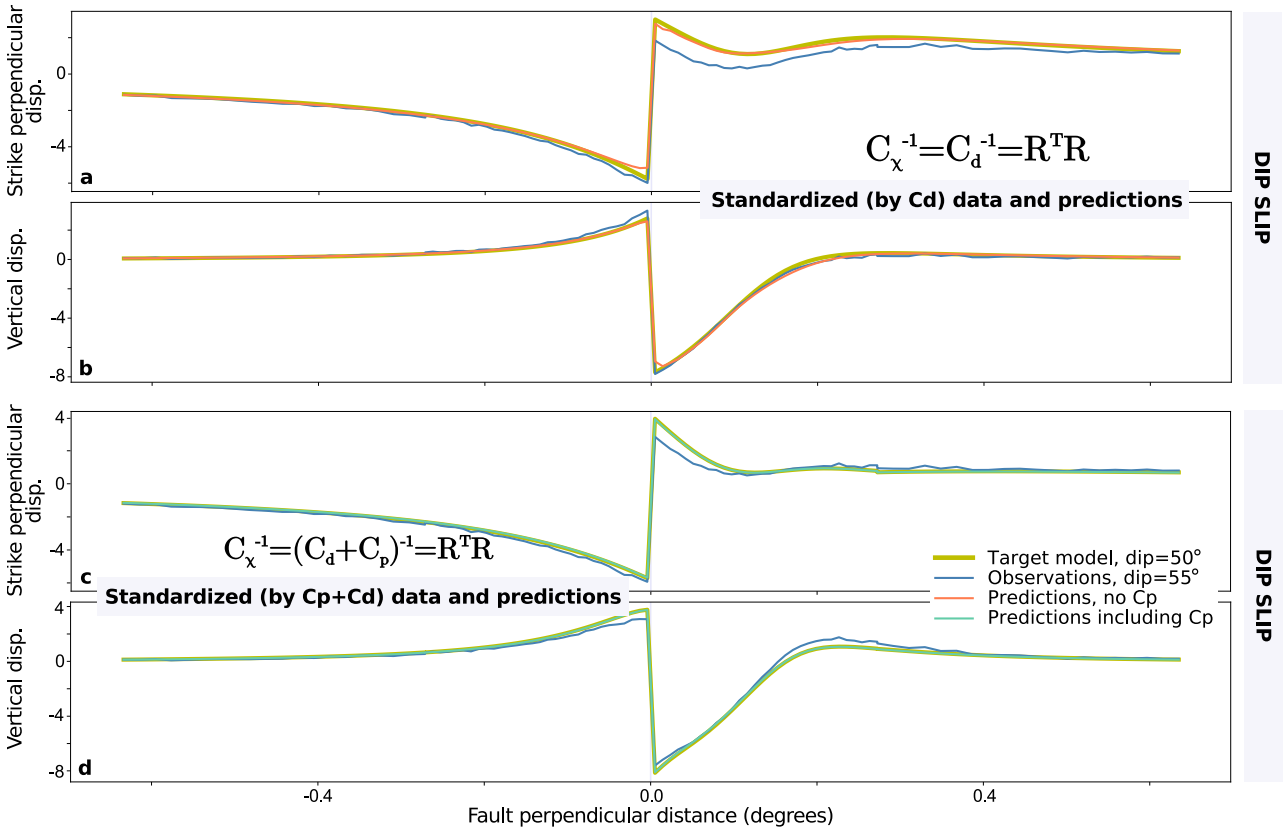

Figure S1 – Comparisons between standardized data and predictions with and without accounting for $\mathbf{C}_\mathrm{p}$, for a fault with dip-slip motion and assuming an incorrect dip angle. The location of the fault surface rupture is shown with gray vertical line. Standardized data and predictions without accounting for $\mathbf{C}_\mathrm{p}$ (i.e. $\mathbf{C}_\chi = \mathbf{C}_\mathrm{d}$) are shown in (a) and (b), respectively for strike perpendicular and vertical surface displacements. Standardized data and predictions accounting for $\mathbf{C}_\mathrm{p}$ (i.e. $\mathbf{C}_\chi = \mathbf{C}_\mathrm{p} + \mathbf{C}_\mathrm{d}$) are shown in (c) and (d). The standardized observations $\mathbf{Rd}_\mathrm{obs}$ (with $\mathbf{C}_\chi^{-1} = \mathbf{R}^T\mathbf{R}$) are shown in blue. The standardized displacements in khaki green are produced by the 1 m uniform target model assuming an incorrect fault dip. The standardized predictions $\mathbf{Rd}_\mathrm{pred}$ shown in orange and green are calculated from the posterior mean model, respectively without and with $\mathbf{C}_\mathrm{p}$ included (and thus with a different $\mathbf{R}$ matrix).

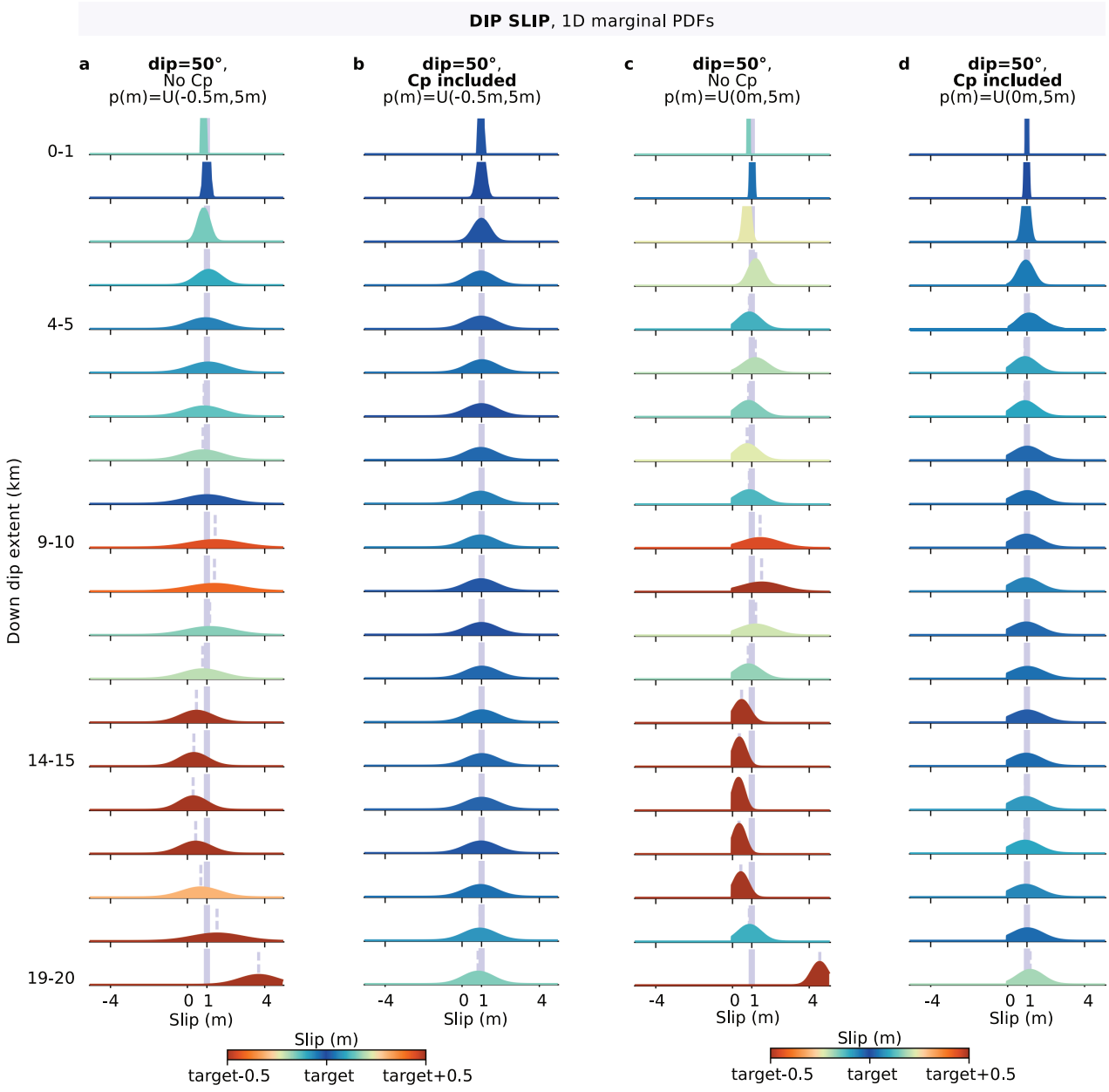

Figure S2 – Comparison of inversion results with and without neglecting the prediction uncertainty, for a dip-slip scenario with varying assumed prior. The uniform target slip model is shown as a grey vertical bar. In (a) and (b), the assumed prior allows for 50 cm of up dip slip, whereas in (c) and (d) the prior is strictly positive. The posterior PDFs are shown in (a) and (c) when the prediction uncertainty is neglected and in (b) and (d) if $\mathbf{C}_\mathrm{p}$ is included in the inversion. The posterior mean model is indicated with a vertical grey dotted line. The offset between target model and posterior mean is displayed with a colorscale saturated at 50cm.

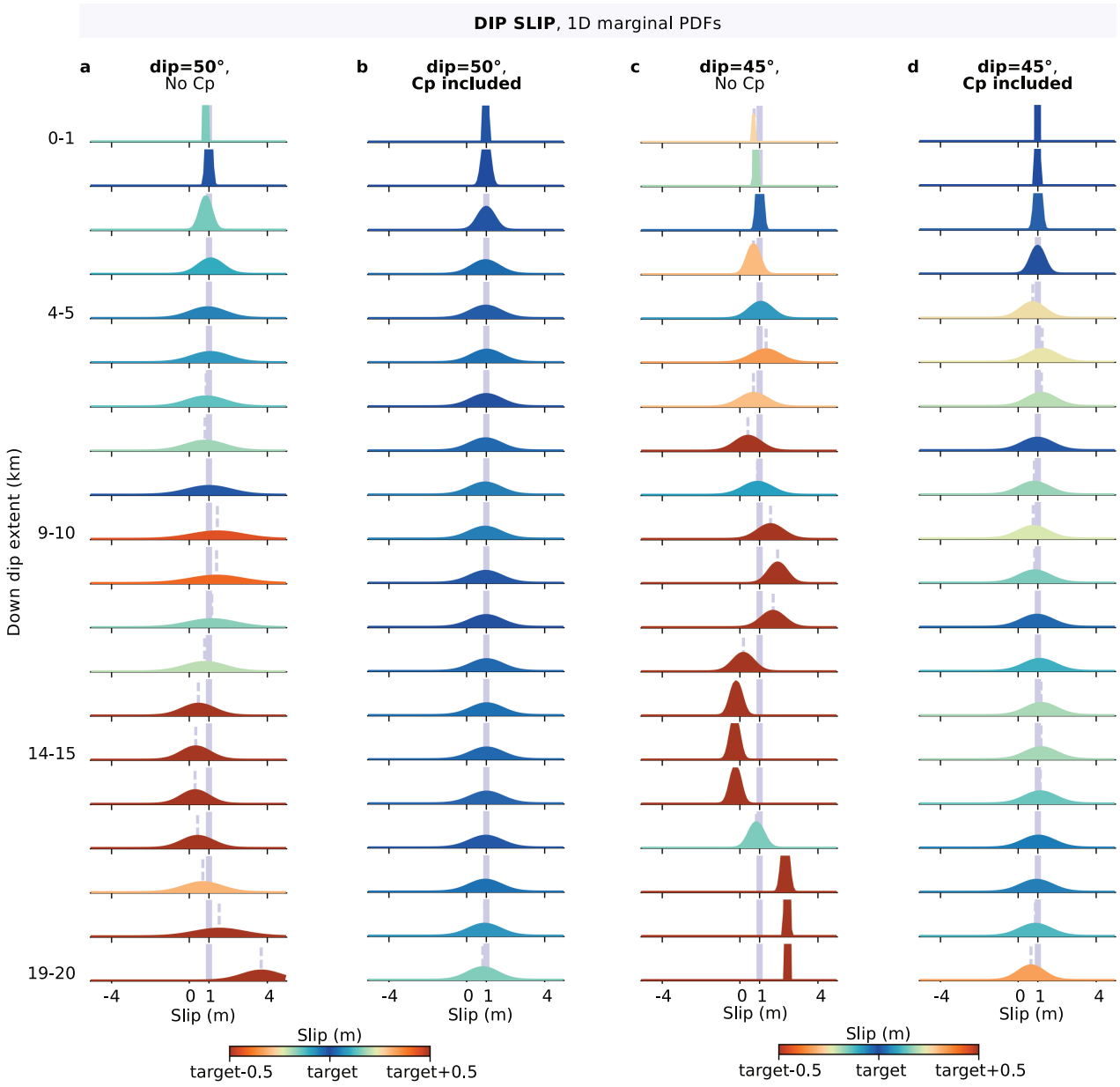

Figure S3 – Comparison of inversion results with and without neglecting the prediction uncertainty, for a dip-slip scenario. The uniform target slip model is shown as a grey vertical bar. The correct fault is of 55° dip, whereas the assumed fault for inversion is of 50° dip in (a) and (b) and of 45° dip in (c) and (d). The posterior PDFs are shown in (a) and (c) when the prediction uncertainty is neglected and in (b) and (d) if $\mathbf{C}_\mathrm{p}$ is included in the inversion. The posterior mean model is indicated with a vertical grey dotted line. The offset between target model and posterior mean is displayed with a colorscale saturated at 50cm.

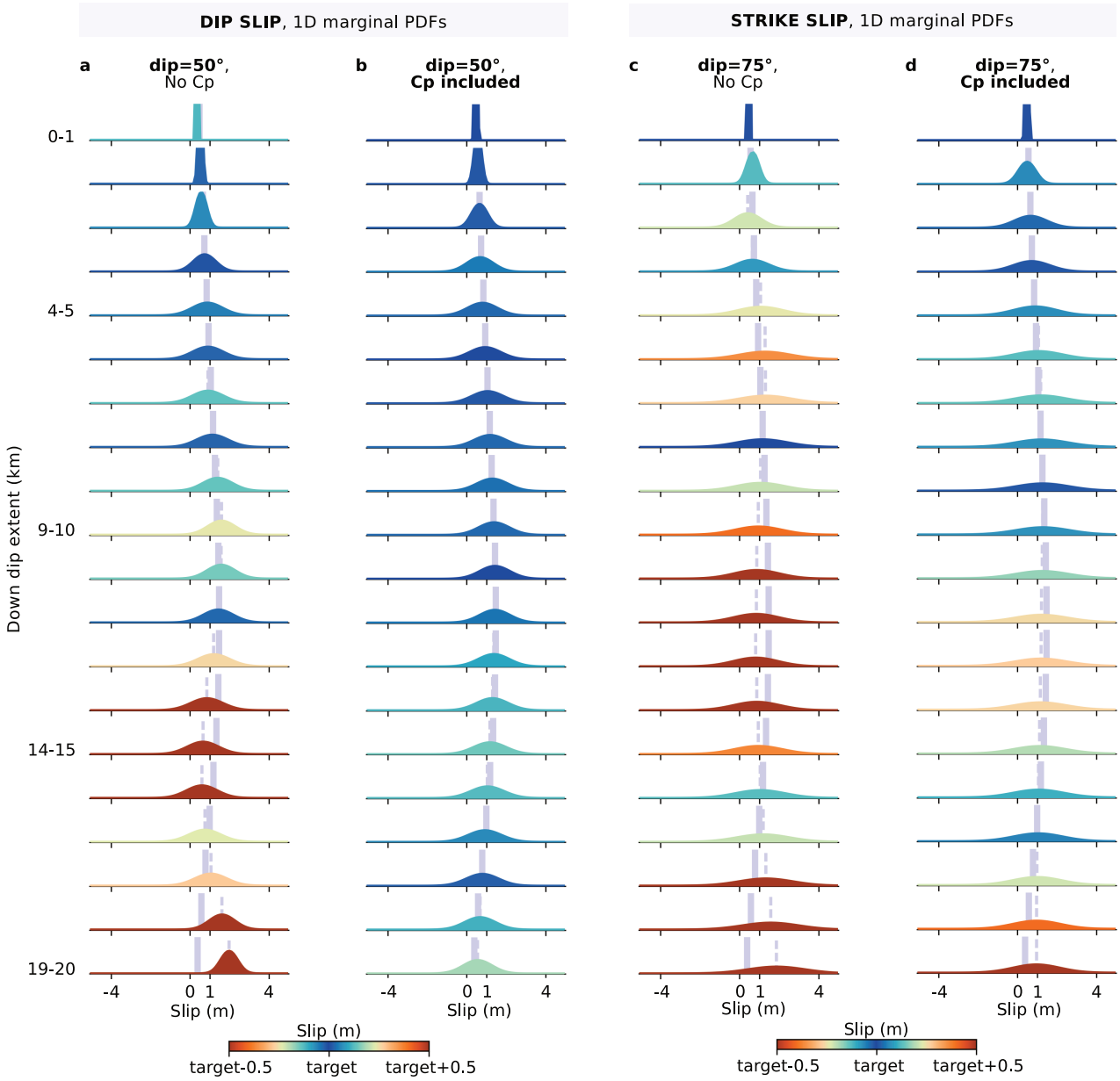

Figure S4 – Comparison of inversion results with and without neglecting the prediction uncertainty. The non-uniform target slip model is shown as a grey vertical bar. The posterior PDFs are shown in (a) and (c) when the prediction uncertainty is neglected and in (b) and (d) if $\mathbf{C}_p$ is included in the inversion, respectively for dip-slip and strike-slip behavior. The posterior mean model is indicated with a vertical grey dotted line. The offset between target model and posterior mean is displayed with a colorscale saturated at 50cm.

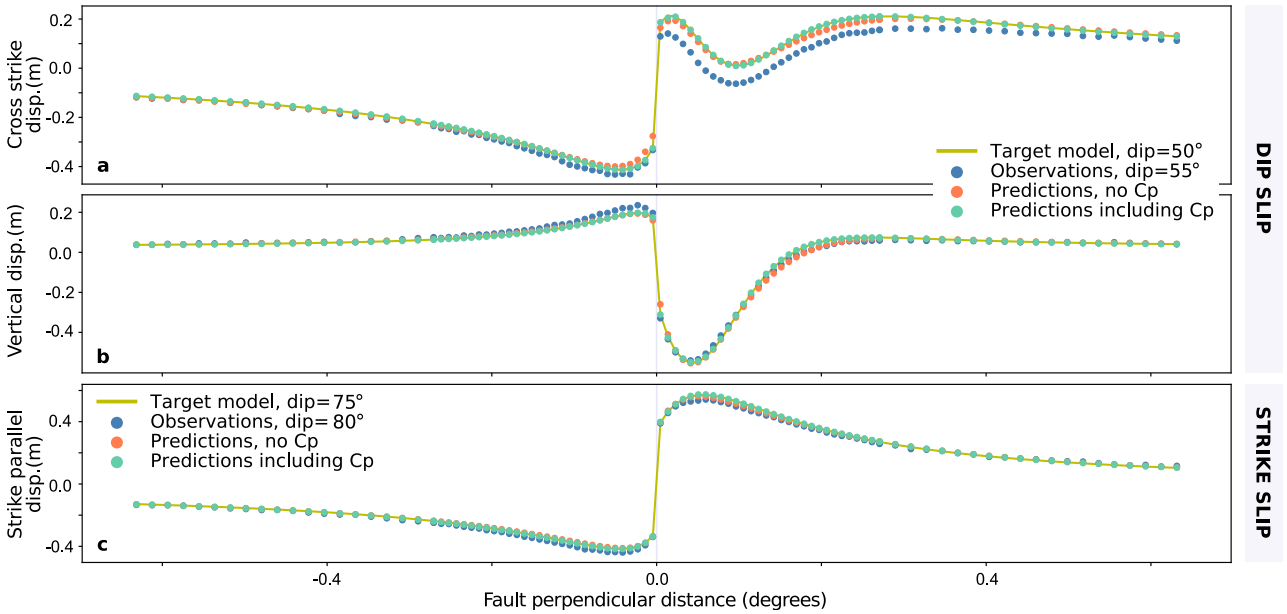

Figure S5 – Comparisons between synthetic data and predictions with and without accounting for $\mathbf{C}_\mathrm{p}$. We assume the slip on the fault to be non-uniform. The location of the fault surface rupture is shown with gray vertical line. Dip-slip behavior (assumed fault dip of 50°) generates cross strike surface displacement (a) and vertical surface displacement (b), whereas strike-slip (assumed fault dip of 75°) behavior produces only strike parallel displacement (c). The data points (i.e. generated by a slip on the true fault) are shown in blue. The displacements in khaki green are produced by the 1 m uniform target model assuming an incorrect fault dip. The predictions shown in orange and green are calculated from the posterior mean model, respectively without and with $\mathbf{C}_\mathrm{p}$ included.

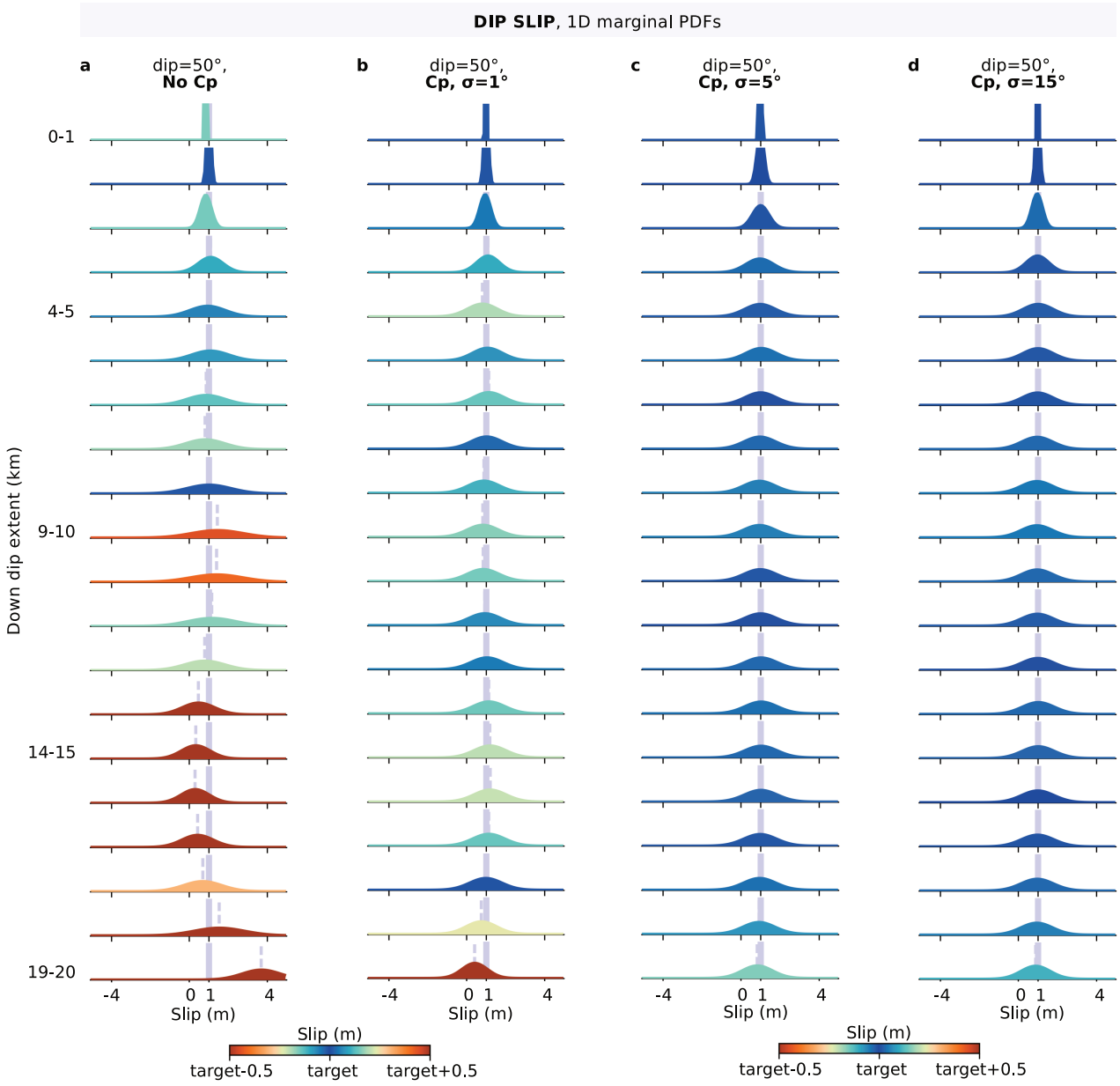

Figure S6 – Comparison of inversion results with or without neglecting for the prediction uncertainty for a dip-slip scenario. The uniform target slip model is shown as a grey vertical bar. The posterior PDFs are shown in (a) when the prediction uncertainty is neglected. When $\mathbf{C}_\mathrm{p}$ is included in the inversion, the assumed standard deviation varies from 1°, 5° to 10° respectively in (b), (c) and (d). The posterior mean model is indicated with a vertical grey dotted line. The offset between target model and posterior mean is displayed with a colorscale saturated at 50cm.

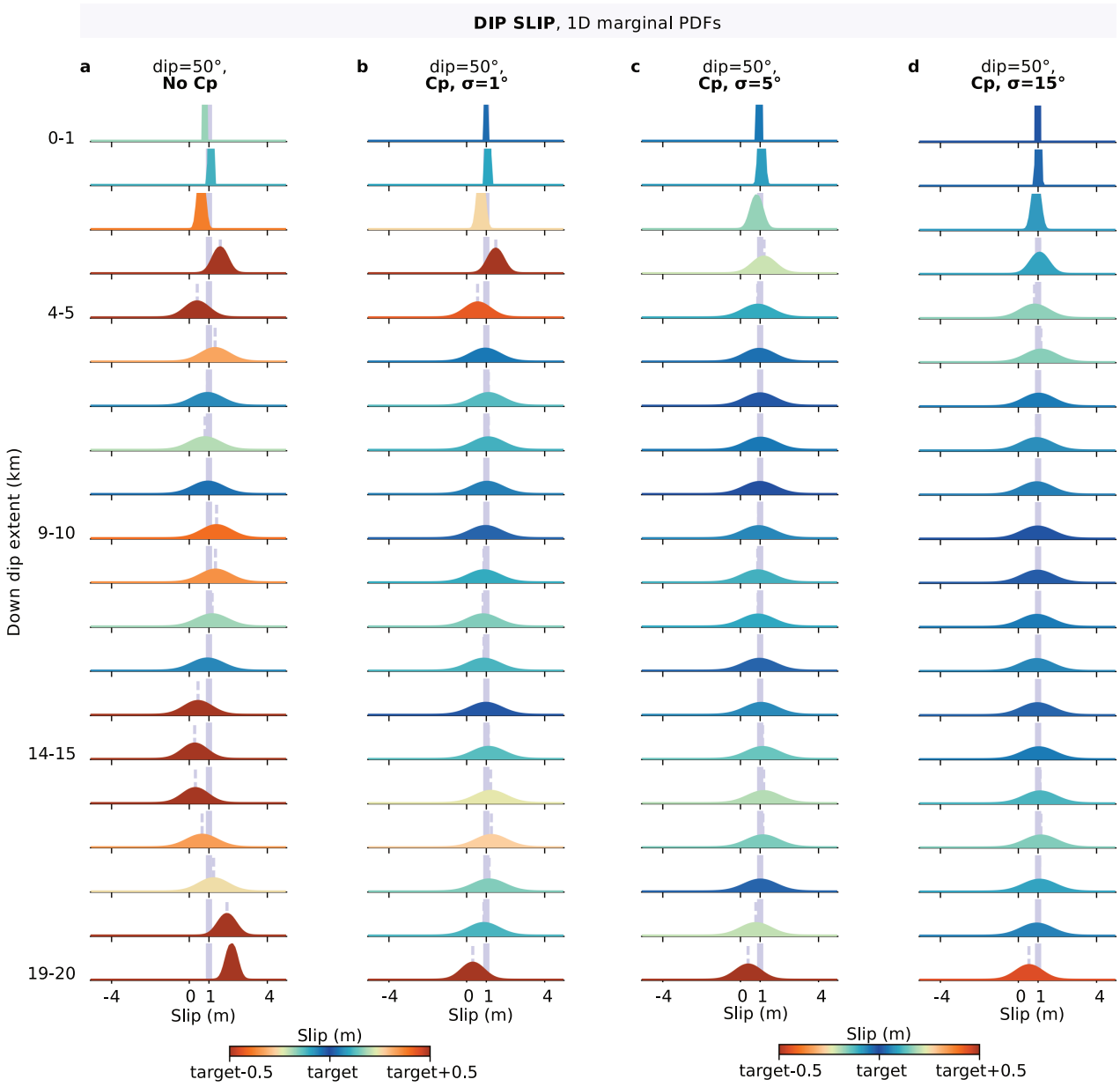

Figure S7 – Comparison of inversion results with or without neglecting for the prediction uncertainty for a dip-slip scenario. The uniform target slip model is shown as a grey vertical bar. The posterior PDFs are shown in (a) when the prediction uncertainty is neglected. When $\mathbf{C}_p$ is included in the inversion, the assumed standard deviation varies from 1°, 5° to 10° respectively in (b), (c) and (d). In this case, the observational errors are assumed of 4 mm, and are thus understimated as the added noise is of 7 mm. The posterior mean model is indicated with a vertical grey dotted line. The offset between target model and posterior mean is displayed with a colorscale saturated at 50cm.

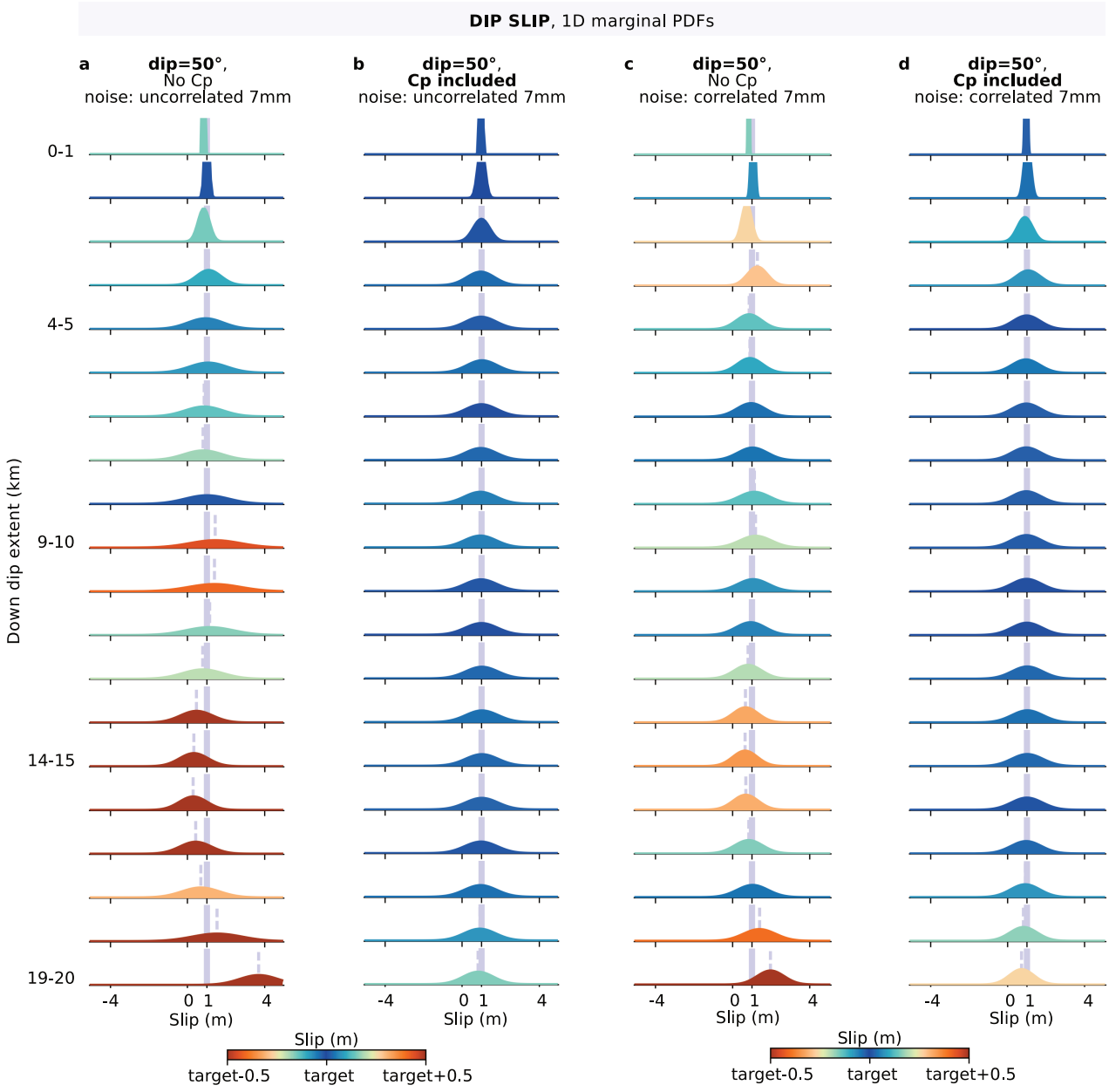

Figure S8 – Comparison of inversion results with or without neglecting for the prediction uncertainty for a dip-slip scenario. The uniform target slip model is shown as a grey vertical bar. The posterior PDFs are shown in (a) and (c) when the prediction uncertainty is neglected and in (b) and (d) if $\mathbf{C}_p$ is included. In (a) and (b), the noise added to the data has an amplitude of 7 mm. In (c) and (d), the noise has an amplitude of 7 mm and is correlated spatially. The posterior mean model is indicated with a vertical grey dotted line. The offset between target model and posterior mean is displayed with a colorscale saturated at 50cm.

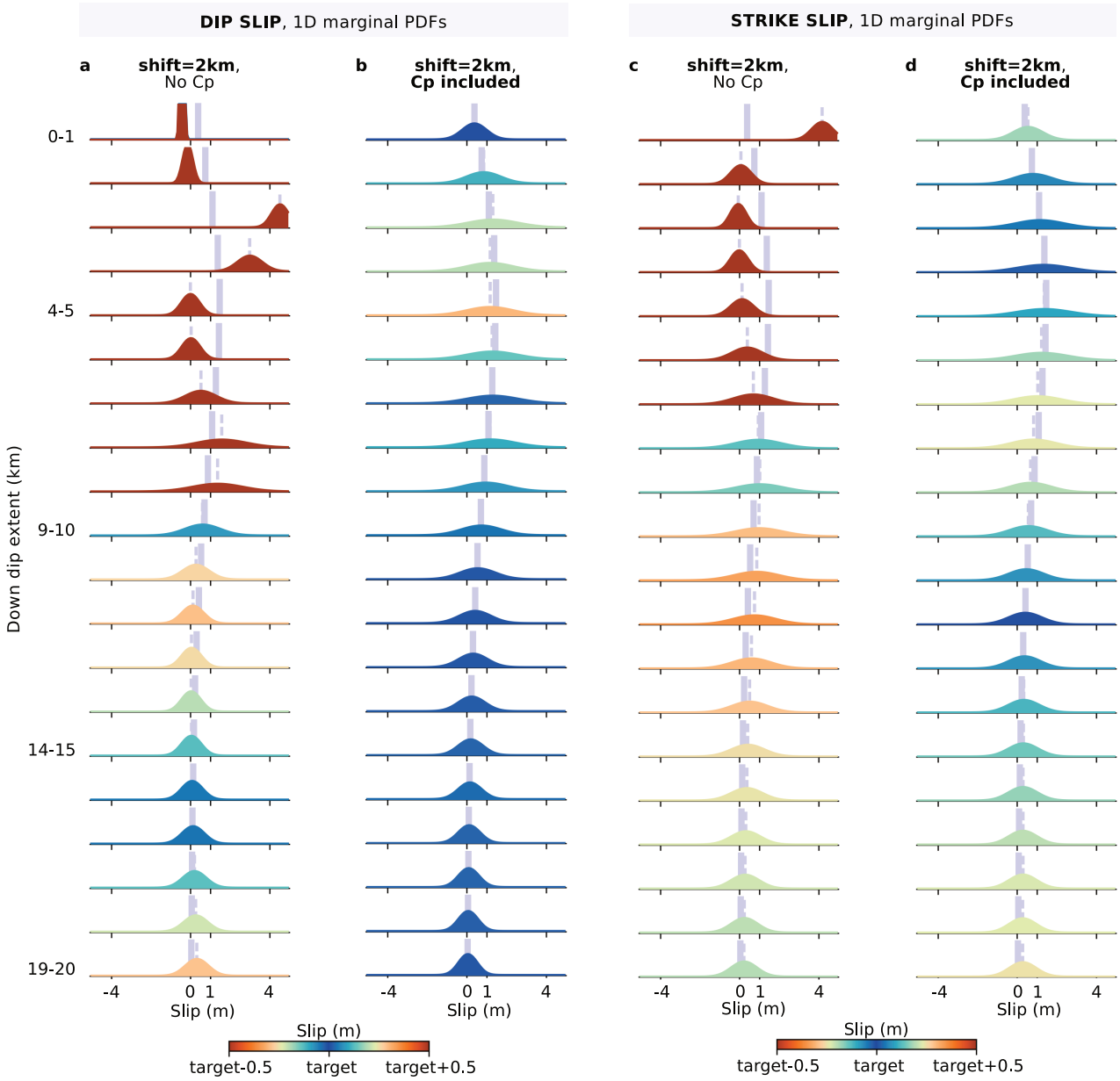

Figure S9 – Comparison of inversion results with and without neglecting the prediction uncertainty. The non-uniform target slip model is shown as a grey vertical bar. The offset between correct and assumed faults is of 2 km. The posterior PDFs are shown in (a) and (c) when the prediction uncertainty is neglected and in (b) and (d) if $\mathbf{C}_\mathrm{p}$ is included in the inversion, respectively for dip-slip and strike-slip behavior. The posterior mean model is indicated with a vertical grey dotted line. The offset between target model and posterior mean is displayed with a colorscale saturated at 50cm.

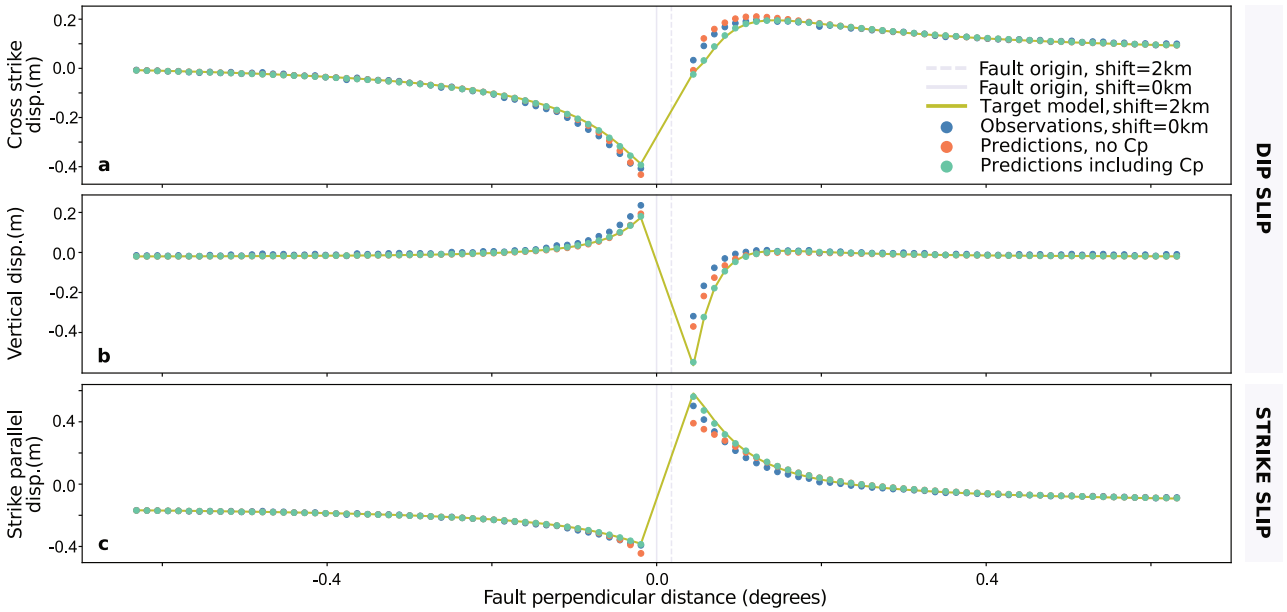

Figure S10 – Comparisons between synthetic data and predictions with and without accounting for $\mathbf{C}_\mathrm{p}$. We assume the slip on the fault to be non-uniform. The correct location of the fault surface rupture is shown with gray vertical line, whereas the assumed fault position is shown by a dotted grey vertical line. Dip-slip behavior generates cross strike surface displacement (a) and vertical surface displacement (b), whereas strike-slip behavior produces only strike parallel displacement (c). The data points (i.e. generated by a slip on the true fault) are shown in blue. The displacements in khaki green are produced by the 1 m uniform target model assuming an incorrect fault dip. The predictions shown in orange and green are calculated from the posterior mean model, respectively without and with $\mathbf{C}_\mathrm{p}$ included. The 5 missing data points around the faults position have been removed to simulate a real case.

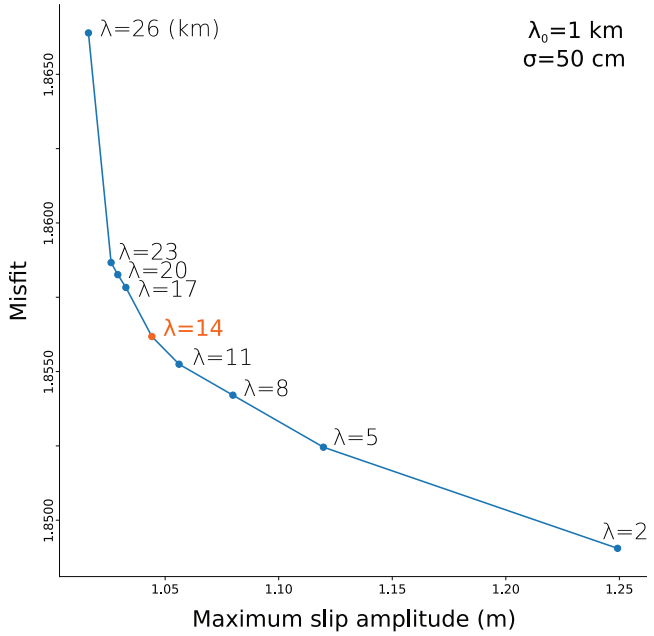

Figure S11 – Misfit (see eq. 1, with $\mathbf{C}_\chi(\mathbf{m}) = \mathbf{C}_\mathrm{d}$) as a function of maximum slip amplitude (indication of model roughness) for different optimizations made assuming correlation lengths varying from 2 to 26 km. We finally assume for our optimizations the value of 14 km. The a priori standard deviation of model parameters σ has been chosen from the posterior standard deviation of model parameters of a Bayesian optimization (see Fig. 5). Our assumed σ is of 50 cm. The scaling factor λ_0 is usually chosen as average distance between subfaults, and is thus assumed here of 1 km.

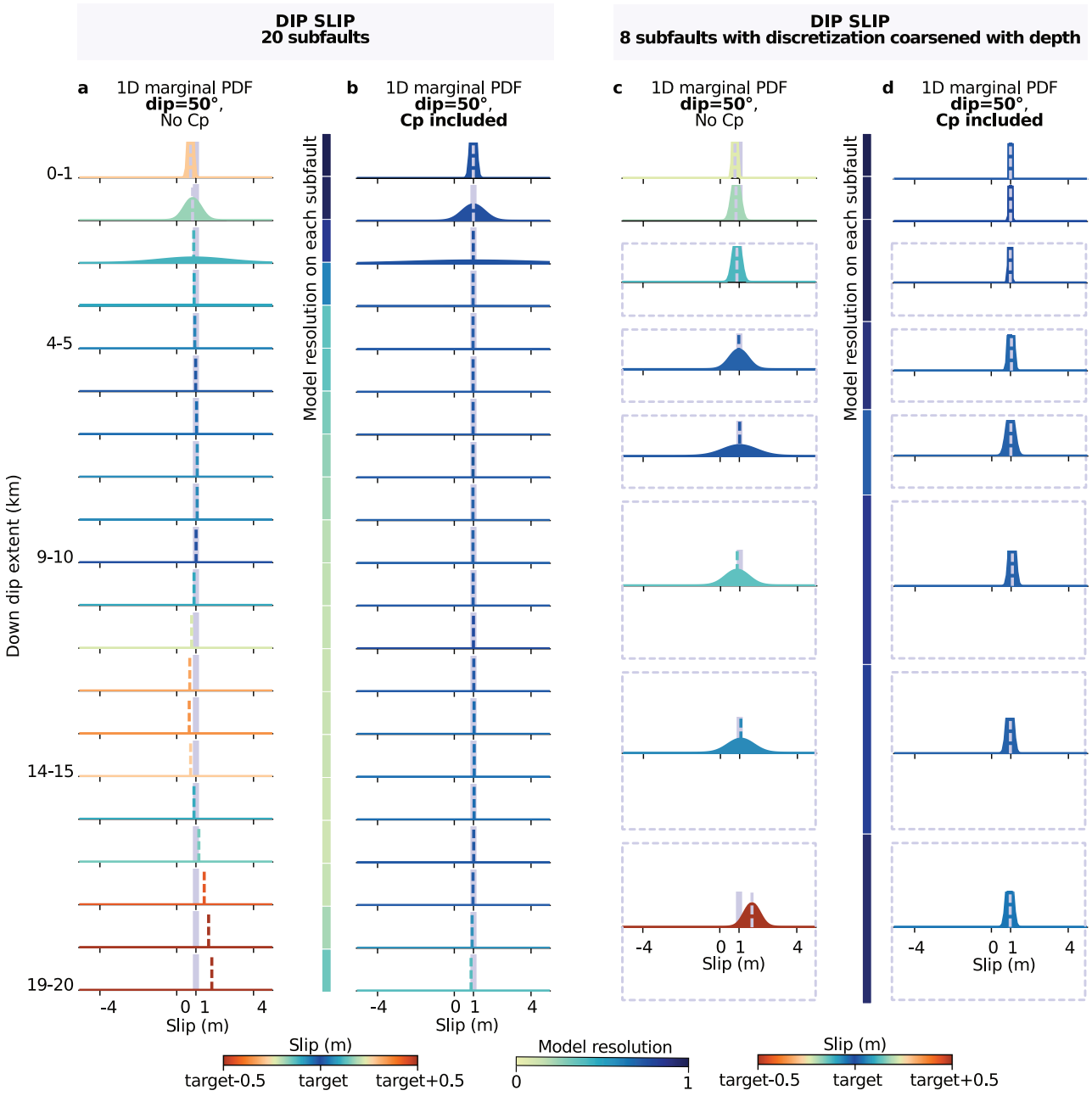

Figure S12 – Comparison of results for a positive least squares optimization, with and without incorporating $\mathbf{C}_\mathrm{p}$. The uniform target slip model is shown as a grey vertical bar. The inversion results are shown in (a) and (c) when the prediction uncertainty is neglected and in (b) and (d) if $\mathbf{C}_\mathrm{p}$ is included in the inversion, respectively for a 20 subfaults or a 8 subfaults fault parametrization. The inferred model corresponds to the mean of the posterior gaussian distribution, the standard deviation being the uncertainty on inferred parameters $\mathbf{C}_\mathrm{m} = (\mathbf{G}^T \cdot \mathbf{C}_\chi^{-1} \cdot \mathbf{G})^{-1}$. The posterior mean model is indicated with a grey vertical dotted line, or with a colored dotted line if the posterior distribution is almost uniform (i.e the posterior uncertainty is high). The offset between target and resulting model is displayed with a colorscale saturated at 50 cm.

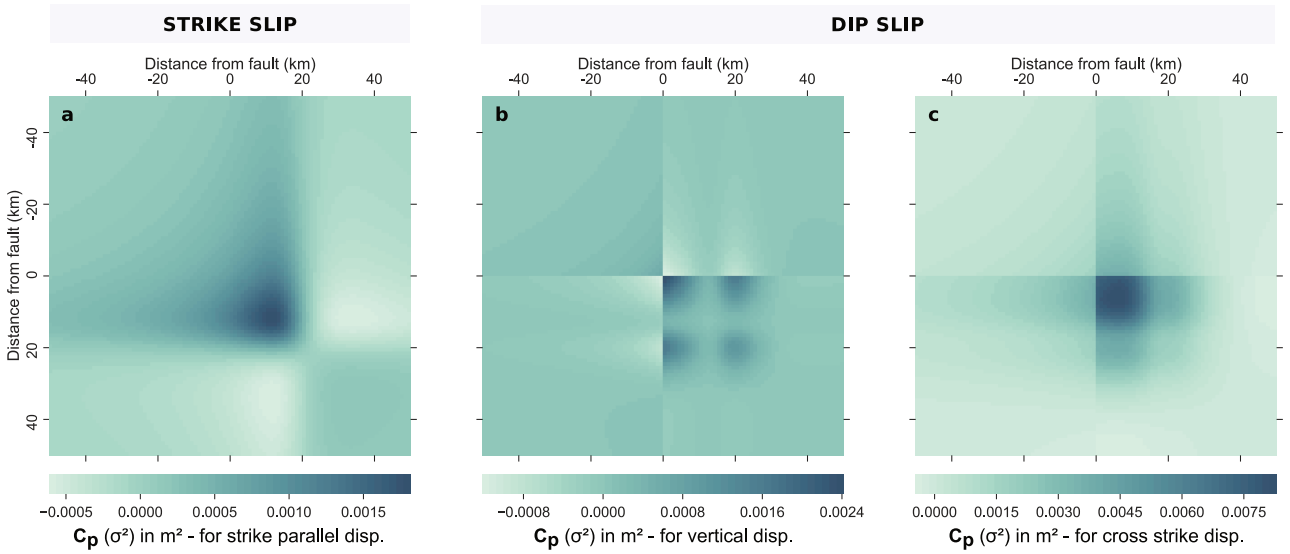

Figure S13 – $\mathbf{C}_\mathrm{p}$ due to imprecise fault dip in a simplified 2D application. The assumed fault does not vary along strike, is 20 km large and is dipping of 35° while the correct fault is dipping 30°. The assumed model $\mathbf{m}_\mathrm{prior}$ is uniform at 1 m. The prediction covariance matrix $\mathbf{C}_\mathrm{p}$ is shown for strike parallel, vertical and cross strike surface displacement respectively in (a), (b) and (c).